Fabrication and Characterization of Thermally Actuated Bimorph Probe for Living Cell Measurements with Experimental and Numerical Analysis

Younghak Cho, Beomjoon Kim
CIRMM, Institute of Industrial Science, The University of Tokyo,
4-6-1 Komaba, Meguro-ku, Tokyo 153-8505, Japan
Seokkwan Hong, Jeongjin Kang*
Korea Institute of Industrial Technology,
#401-301, Bucheon TP, 193, Yakdae-dong, Wonmi-gu, Bucheon, Kyunggi-do 420-734, Korea

This paper deals with a novel structure for single-cell characterization which makes use of bimorph micro thermal actuators combined with electrical sensor device and integrated microfluidic channel. The goal for this device is to capture and characterize individual biocell. Quantitative and qualitative characteristics of bimorph thermal actuator were analyzed with finite element analysis methods. Furthermore, optimization for the dimension of cantilevers and integrated parallel probe systems with microfluidic channels is able to be realized through the virtual simulation for actuation and the practical fabrication of prototype of probes. The experimental value of probe deflection was in accordance with the simulated one.

Key Words : Bimorph Thermal Actuator, Single-cell Measurement, SU-8

Nomenclature

V : is the nodal voltage vector
T : is the nodal temperature vector
u : is the nodal displacement vector
$K_E(T)$: is the temperature-dependent electrical conductivity matrix
I : is the nodal current vector
$C_T(T)$: is the temperature-dependent heat capacity matrix
$K_T(T)$: is the temperature-dependent thermal conductivity matrix
Q : is the heat flux vector
Q_E : is the heat generation due to electrical flow vector
Q_I : is the heat generation due to inelastic deformation vector
Q_F : is the heat generation due to friction vector
M : is the mass matrix
D : is the damping matrix
$K_M(T,u,t)$: is the temperature, deformation and time-dependent stiffness matrix
F : is the externally applied force vector
F_T : is the force due to thermal strain vector

* Corresponding Author,
E-mail : doublej@kitech.re.kr
TEL : +82-32-234-0603; **FAX** : +82-32-234-0607
Korea Institute of Industrial Technology, #401-301, Bucheon TP, 193, Yakdae-dong, Wonmi-gu, Bucheon, Kyunggi-do 420-734, Korea. (Manuscript **Received** May 2, 2005; **Revised** January 12, 2006)

1. Introduction

In the past few years, the interest in analysis of even more complex biological systems such as living cells with the use of microfabricated structures has attracted increased attention. Thus, the application of microfabricated techniques (MEMS techniques) has really entered the life science field and has started to serve as a driving force for discover in cell biology, neurobiology, pharmacology, and tissue engineering. Specially, single-cell analysis and manipulation have been highly pursued by biologists over the past decade, be-

cause microanalysis systems and biosensing systems based on single cell make it possible to perform analysis for a wide range of applications from fundamental biology research to drug development.

The development of tools for single-cell manipulation and characterization in aqueous media is of major importance for the rapidly growing area of cellomics as well as genomics and proteomics. Specially, using microactuator is very useful for single-cell manipulation. To manipulate individual cell, the micro gripper devices operating in an aqueous environment using SU-8 was also introduced by Chronis and Lee (2004). However, this device cannot be used for the characterization of cells.

Also, detection as well as manipulation of individual cell in microfluidic channel on chip (flow cytometry) is possible through the microactuator and widely used. Recently, it is possible to measure the mechanical properties of the living biological samples (such as the cell-to-cell interaction force and elastic property of cell itself) in aqueous media with the AFM (Fadmacher, 1997). Similar to the force measurement of cell in single level using AFM, three-dimensional movable microsensor with vertical probe actuation, which can isolate the cell from environment, makes it possible to characterize the electrical property as well as mechanical property of cell.

Some simulated results on thermally actuated MEMS devices were introduced (Pichonat-Gallois and Labachelerie, 2003; Yu and Yang, 2003). However, these simulated results are in agreement with experimental results for low temperature range, but high difference between them appears as the temperature is going up. It may be due to the fact that they did not consider the material properties dependent on temperature, and that conduction and convection were underestimated. Therefore, the heat generation and loss should be in detail investigated to describe the actuation characteristics of bimorph thermal actuator exactly.

We introduced a novel device for a single-cell characterization (Kim et al., 2003). In this device, we used the doped poly-silicon, which is well adapted to measure electrical signal. Also, the difference of thermal expansion coefficients between poly-silicon and transparent photo-plastic material (SU-8) is used as the main advantage for bimorph actuation of the sensing probes. SU-8 follows surface contours conformal down to the nanometer range and is easily covered to poly-silicon probe structure inside micro channel. The device can be also optically monitored when capturing small objects even if located under the poly-silicon cantilevers.

In this research, we present the details of the fabrication of bimorph thermal actuators combined with electrical sensor device and integrated micro-fluidic channel in order to realize cell manipulation and electrical detection. Moreover, quantitative and qualitative characteristics of bimorph micro actuator are investigated with finite element analysis methods. Through the virtual simulation, we can get information about actuation characteristics for optimization of bimorph thermal actuator.

2. Fabrications

The schematic view of the device is shown in Fig. 1. The device consists of three independent

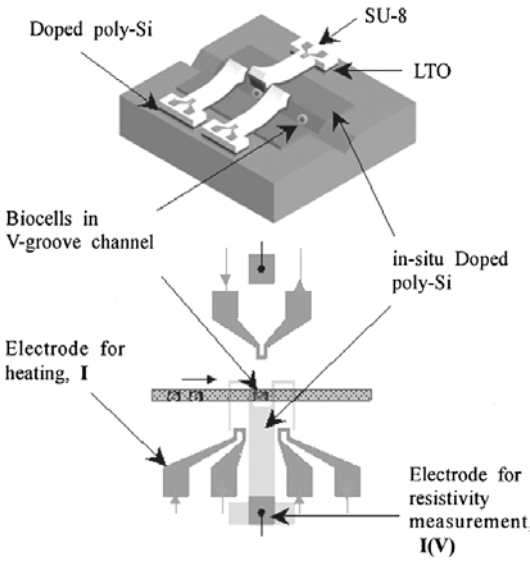

Fig. 1 Schematic view of cell capture and electrical measurement

self-actuated probes on the fluidic channel. The middle positioned probe is actuated to immobilize individual biocell and measure electrical characterization of it simultaneously, while other two probes are actuated to open and close the flow of cells for capturing.

The fabrication process is like the followings. The V-grooves for microfluidic channel as well as micro-mold for tip formation of the sensor part of the probe arrays are fabricated by anisotropic KOH etching, and then deposited with SiN for insulation. After in-situ doped poly-silicon and low temperature oxide (LTO) are deposited, 2 μm poly-silicon is deposited, doped by phosphorus implantation and finally annealed. The poly-silicon is patterned by photolithography and etched by RIE (SF_6 and CF_4 gas), and then transparent photo-plastic material (SU- 8) is also patterned for cantilever structures. The probe cantilevers are made with conjugation of doped-poly-silicon, SU-8. The patterned Cr/Au electrodes for heating of poly-Si/SU-8 cantilevers are covered with very thin SU-8 (less than 800 nm in thick) to prevent metal layers from peeling-off. Finally, poly-Si/SU-8 cantilevers are released from the fluidic channel when the sacrificial layer of LTO is etched by BHF solution. Figure 2 shows the whole device integrated with the flow channel and probe cantilever as well as inlet.

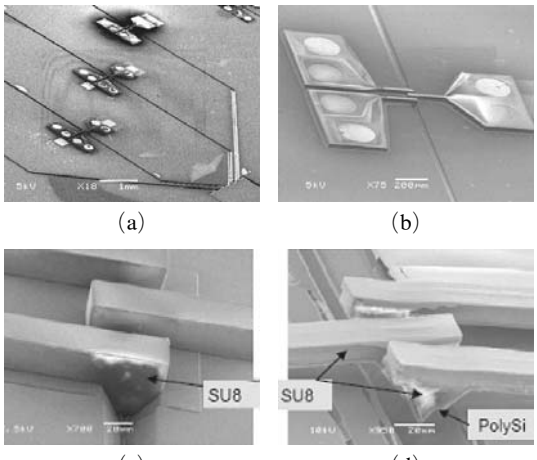

Fig. 2 SEM images of probe arrays with microfluidic channel and probe cantilevers. (c) before release. (d) after release

3. Operation Principle and Method

Usually, a bimorph actuator is composed of two thin panels of ceramic elements bonded together with a flexible metallic panel as its central electrode. By wiring these two elements in such a way as to make one elongate and the other contract by applying voltage, inflection deviation occurs conforming to the waveform of the applied voltage. This allows it to be used as an actuator.

When the probes are released by sacrificial layer etching, probe cantilevers in length of 250 μm are bent up to around 30 μm due to residual stress between SU-8 (20 μm thick) and poly-silicon cantilever structures (2μm thick) as shown in Fig. 2. When an input voltage is supplied through Au electrodes and the cantilever is heated from top side, temperature rise provides beam bending down due to the difference between the coefficients of thermal expansion of SU-8 and poly-silicon, and the initial stress.

4. Considerations of Heat Transfer Modes

As shown in Fig. 3, the heat generated by Au electrode is not only conducted to each layer but also transmitted to surroundings by convection and radiation on the structure surface. When Joule heating rate in Au electrode is same to the heat out-flux by conduction, convection and radiation, the system comes to thermal equilibrium state and bimorph thermal actuator shows out-

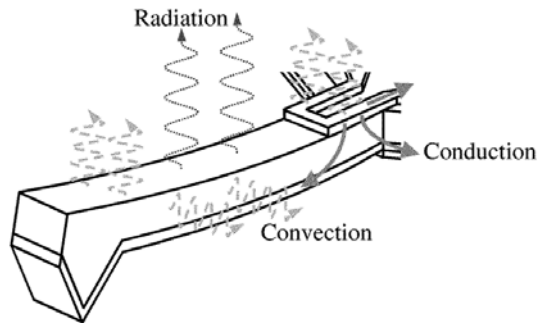

Fig. 3 Heat transfer mechanisms by conduction, convection and radiation

of-plane deflection as mechanical response according to thermal strain distributions at thermal equilibrium state. In this paper, we just consider the area of Au electrode which is top side of probe cantilever.

Before virtual simulation based on finite element analysis, we infer respective effects of heat transfer modes on bimorph thermal actuator from continuum-based theoretical equations (Incropera and De Witt, 1990).

4.1 Joule heating generation

Au electrode deposited on SU-8 structure plays a role of heat source, and related equation is expressed as following.

$$Q_E = VI = \frac{V^2}{R} \tag{1}$$

$$R = \frac{\rho_E L}{A} \tag{2}$$

where Q_E is the Joule heat, V, the supplied voltage, I, the current, R, the resistance, ρ_E, the electrical resistivity, L, the length of electrode, and A, the cross section area of electrode. Electrical resistivity is a variable material property as temperature changes. Therefore, resistance of the narrowest Au electrode area on probe cantilever is just calculated to be around 8.1, 13.0, 18.2 Ω when the electrode temperature is assumed to be uniformly 600, 900, 1200 K. When 1 V is supplied to Au electrode, Joule heat of around 123, 77, 55 mW is generated.

4.2 Conduction

Most of heat generated by Au electrode on top of cantilever is transmitted to Au electrode of probe body and SU-8 structure by conduction. Heat transfer rate by conduction is expressed as well-known Fourier's law.

$$q''_{cond} = -k \frac{dT}{dx} \tag{3}$$

where q''_{cond} is the heat transfer rate in the x direction per unit area perpendicular to the direction of transfer, k, the thermal conductivity, and dT/dx, the temperature gradient.

Under proper assumption that temperature of Au electrode is 600, 900, 1200 K and temperature of surroundings separated from Au electrode is 300 K, heat transfer rate conducted along with Au electrode and heat transfer rate transmitted to SU-8 are about 11, 20, 29 mW and 5, 10, 15 mW, respectively.

4.3 Convection

q''_{conv}, the convective heat flux is expressed as Newton's law of cooling.

$$q''_{conv} = h(T_s - T_\infty) \tag{4}$$

where T_s and T_∞ are the surface and fluid temperatures, respectively. The proportionality constant h as the convection heat transfer coefficient is averagely determined as follows.

$$\bar{h} = \overline{Nu}_L \frac{k_F}{L} \tag{5}$$

where $\overline{Nu}_L$ is the average Nusselt number, k_f, the thermal conductivity of the fluid, and L, the characteristic length.

Because the characteristic length L is very small, $\bar{h}$ has higher value than that in macro scale by size effect. When it is assumed that T_s, is 600, 900, 1200 K, and T_∞ is 300 K, respectively, is around 550, 690, 794 W/m^2·K and convection heat transfer rate is 0.14, 0.35, 0.60 mW. The role of convection in heat transfer at high temperature becomes important because the thermal conductivity of air, k_t, is in proportion to temperature. The thermal conductivity of air as a function of temperature at atmospheric pressure is given by Vargaftik (1956).

4.4 Radiation

q''_{rad}, the net rate of radiation heat exchange between the surface and its surroundings, per unit area of the surface, is assumed as follows.

$$q''_{rad} = \varepsilon\sigma(T_s^4 - T_{sur}^4) \tag{6}$$

where ε is the emissivity, σ, the Stefan-Boltzmann constant, and T_{sur}, the temperature of the surroundings.

Assumed that T_s, T_{sur} are 600 K, 300 K, respectively, radiation heat transfer rate on the Au electrode surface (emissivity, ε=0.04) is 2.3×10^{-4} mW. When T_s is assumed to be 900, 1200 K, radiation heat transfer rate is 1.2×10^{-3}, 3.9×10^{-3}

mW. Heat loss by radiation can be neglected, because it is very small when compared with heat emission by conduction or convection (Kim et al., 2002).

4.5 Discussion

Tables 1~3 show the comparison between heat transfer modes (conduction, convection, radiation) for different temperature of Au electrode, respectively. All of these are calculated from Eqs. (1)~(6).

As the temperature of Au electrode rises by Joule heating, the resistance of Au electrode also grows high. It results in reduction of heat generating rate, and the reduction of heat generating rate affects the increase of heat transfer rate transmitted to surroundings. Moreover, increase of temperature causes increase of convection heat transfer coefficient, because the average Nusselt number in Eq. (5) does not almost change but the thermal conductivity of air, k_t, increase 2~3 times. Therefore, the role of convection in heat transfer becomes important (Kim et al., 2002).

Table 1 Comparison between heat transfer modes (T_{Au}=600 K)

Heat generation rate		0.123W	—
Heat transfer rate by	conduction	0.016W	99.13%
	convection	0.00014 W	0.87%
	radiation	2.3×10^{-7}W	~0.00%
Total heat transfer rate		0.01614W	100.00%

Table 2 Comparison between heat transfer modes (T_{Au}=900K)

Heat generation rate		0.077 W	—
Heat transfer rate by	conduction	0.030W	98.85%
	convection	0.00035W	1.15%
	radiation	1.2×10^{-6}W	~0.00%
Total heat transfer rate		0.03035W	100.00%

Table 3 Comparison between heat transfer modes (T_{Au}=1200K)

Heat generation rate		0.055W	—
Heat transfer rate by	conduction	0.044W	98.65%
	convection	0.00060W	1.35%
	radiation	3.9×10^{-6}W	~0.00%
Total heat transfer rate		0.04460W	100.00%

Whether it is valid to consider convection through simulations or not should be discussed.

5. Analysis of Bimorph Thermal Actuator by FE Modeling and Simulation

It is difficult to measure the properties like stress, strain, temperature and so on, because the cantilever size of bimorph thermal actuator is very small (width 30 μm, thickness 22 μm, length 250 μm). That is, it is not easy to analyze the actuation of bimorph thermal actuator fully through experiment. Through virtual simulation, however, it is possible not only to get quantitative and qualitative analysis results, but also to optimize the dimension of cantilevers and integrated parallel probe systems with microfluidic channels.

5.1 Problem definition

Figure 4 shows three-dimensional model of

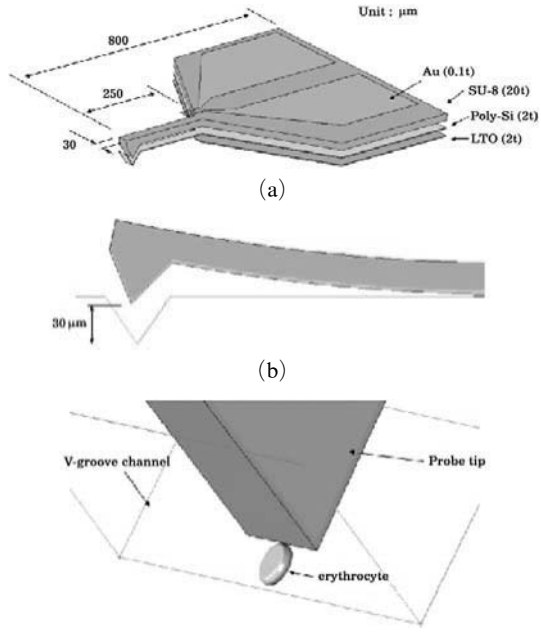

Fig. 4 Three-dimensional model of a bimorph thermal actuator for numerical simulation, (a) Geometry and dimensions with straight beam, (b) Side view of the operated part, (c) Schematic view of the probe tip on an erythrocyte

bimorph thermal actuator for numerical simulation. The respective thickness of four layers and the shape of probe are shown in Fig. 4(a). When the actual probe was released by sacrificial layer etching, probe cantilever in length of 250 μm was bent up to around 30 μm because of residual stress. For considering this bent-up shape at simulation, we gave the change of temperature to the preliminary model of straight beam shape and initial geometry was modeled as shown in Fig. 4 (b). The schematic view of simulation for characterization of an erythrocyte is shown in Fig. 4(c).

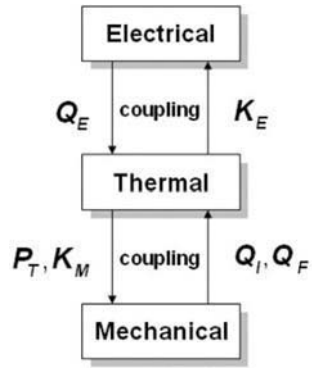

Fig. 5 Coupled electrical-thermal-mechanical analysis

5.2 E-T-M coupled problem

There are many physical phenomena which are deeply related to various physical fields, and the problems in this research also conform to E-T-M (electrical-thermal-mechanical) coupled problems. MSC.MARC was used, which is commercial analysis program, for virtual simulation.

The variations of physical properties of materials were considered along with temperature change, for example, thermal conductivity, electrical resistivity, specific heat, and elastic modulus (Weast et al., 2003 ; 2004). Transient response in heat transfer is reflected along with time, but the solution for mechanical response was obtained under the assumption of quasi-static process. This consideration for conduction and convection is based on heat transfer model in continuum of macro scale, but radiation effect is not taken into account.

Coupling between electrical and thermal problems is mainly caused by heat generation due to electrical flow, Q_E (Joule heating). The thermal and mechanical problems are coupled through thermal strain loads, F_T and heat generation due to inelastic deformation, Q_I and friction, Q_F. Additional coupling may be introduced in case of temperature-dependant electrical conductivity, K_E and mechanical stiffness, K_M. Figure 5 shows the relationships between each physical analysis of one's own.

Nonlinearities may arise in the thermal problem because of convection, radiation, and temperature-dependant thermal conductivity and specific heat. The mechanical problem may also involve geometric and material nonlinearities. Contact is another source of nonlinearity. If contact occurs between deformable and rigid bodies in the mechanical problem, boundary conditions of electrical and thermal problems must be updated to reflect the new contact conditions. In this research, it is, however, assumed that heat generation by deformability or friction is not considered, and that contact between probe and channel does not affect initial boundary conditions.

The matrix equations governing the electrical, thermal and mechanical problems can be expressed as

$$K_E(T)\,V = I \tag{7}$$

$$C_T(T)\,\dot{T} + K_T(T)\,T = Q + Q_E + Q_I + Q_F \tag{8}$$

$$M\ddot{u} + D\dot{u} + K_M(T,\,u,\,t)\,u = F + F_T \tag{9}$$

5.3 FE modeling and material properties

Because the problems in this research include E-T-M coupled response, it is very difficult to make exact modeling considering all conditions. Therefore, we carried out the simulation under proper assumptions.

The material properties used in simulation are shown in Table 4. The variation of physical properties of Au was considered along with temperature change, because Au electrode, which acts as heat source, has wide-ranged temperature change from normal temperature to around melting point.

Table 4 Material properties

Property	Unit	Au	SU-8	Poly-Si	SiO_2
Elastic modulus	GPa	78.5	4.95*	160	73
Poisson's ratio	-	0.42	0.22	0.2	0.17
Mass density	$\times 10^3$ kg/m^3	19.32	1.195	2.33	2.2
Thermal Expansion Coeff.	$\times 10^{-6}$/K	14.1	21*	2.4	0.4
Thermal Conductivity	W/m·K	317*	0.2	30~35	1.32
Specific Heat	J/kg·K	129*	1,200†	753	700
Electrical Resistivity	Ω·m	2.271×10^{-8}*	$10^{12}\sim10^{13}$†	2×10^{-4}	10^{16}

*Given at room temperature (~300 K) and varies along with temperature change
†Presumed value

As shown in Fig. 6(a) and 6(b), variation of thermal conductivity, electrical resistivity, and specific heat of Au along with temperature change was considered. Because the layer of SU-8 is thicker than that of other materials (Au, poly-Si, LTO), SU-8 plays an important role for generation of mechanical bending force. Therefore, variation of elastic modulus along with temperature change was considered about only SU-8 as shown in Fig. 6(c). We did not consider the phase change for all materials along with temperature change. Transient response in heat transfer was reflected along with time, but the solution for mechanical response was considered under quasi-state. The residual stress which is the reason of pre-bending was not considered, assumed that the stress distribution is initialized to zero. The consideration for conduction and convection was based on heat transfer model in continuum of macro scale, but radiation effect was not taken into account.

The boundary temperature between surroundings and LTO layer which plays a role of heat sink by thermal conduction was fixed to 300 K. It is assumed that heat transfer coefficient by convection is 400 W/m^2·K, and that heat transfer coefficient on the surface of Au electrode is specially 1,000 W/m^2·K when considering the high temperature of the surface.

The simulation for actuation was performed for 0.1 sec in real time. 1 V voltage was supplied to Au electrode for first 0.05 sec, and then the current was switched off for the second half. The time interval per increment was 2×10^{-4} sec, so analyses for 500 increments was carried out. For more exact analysis, we tried 2×10^{-5} sec as time

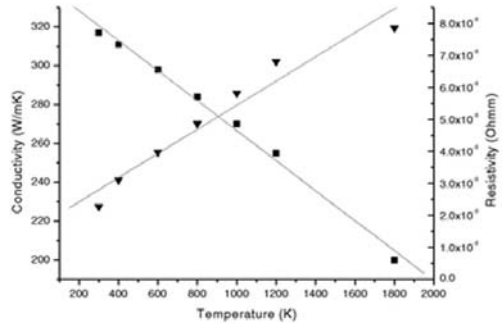

(a) Thermal conductivity and resistivity of Au

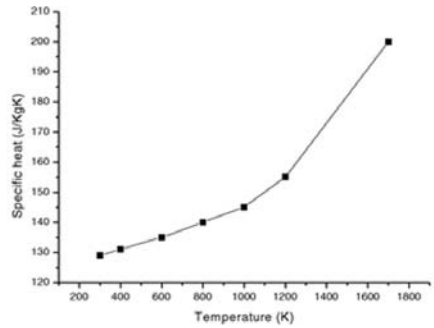

(b) Specific heat of Au

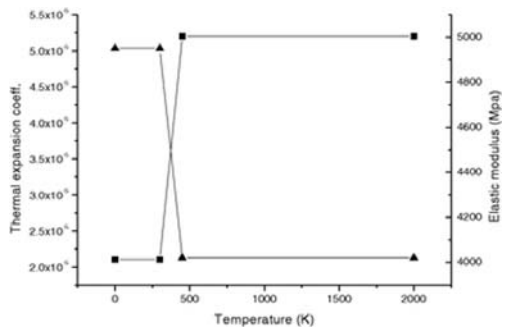

(c) Thermal expansion coefficient and E of SU-8

Fig. 6 Variations of material properties along with temperature change, as inputs for virtual simulations

interval per increment, but we confirmed that there was almost no change for the predicted solutions at steady state.

5.4 Results and discussions

5.4.1 Temperature distribution

Figure 7(b) shows the predicted results of temperature histories at the specific points which are shown in Fig. 7(a). It is predicted that temperature in Au electrode surroundings will come to the 99.5% level of maximum temperature (~1513 K) at steady state within 0.02 sec, and that thermal steady state over whole structure will be realized in 0.05 sec. The melting point of pure Au is around 1337 K (1064℃), and the predicted maximum temperature of Au in simulation was 1513 K. If the predicted temperature is exact, the fabricated probe device cannot work, but real prototype of probe device worked well under same condition. This result means that the physical properties of materials have limits in prediction for actuation of bimorph thermal actuator. When current is switched off, it is expected that the temperature over whole structure will go down under 500 K during 0.004 sec (at 0.054 sec), and that whole physical variables over 99% will return to initial state after 0.05 sec (at 0.1 sec).

Figure 7(c) and 7(d) show the predicted time histories of temperature in case of neglecting convection and in thermally insulated condition, respectively. The predicted temperature at point A at 0.05 sec is around 1600 K and 1658 K, respectively, and moreover at this time the temperature does not arrive at the steady state yet. This result is very different from the result that the maximum temperature at steady state in case of considering convection is 1513 K. During natural cooling after 0.05 sec, temperature histories are also different from those in case of considering convection.

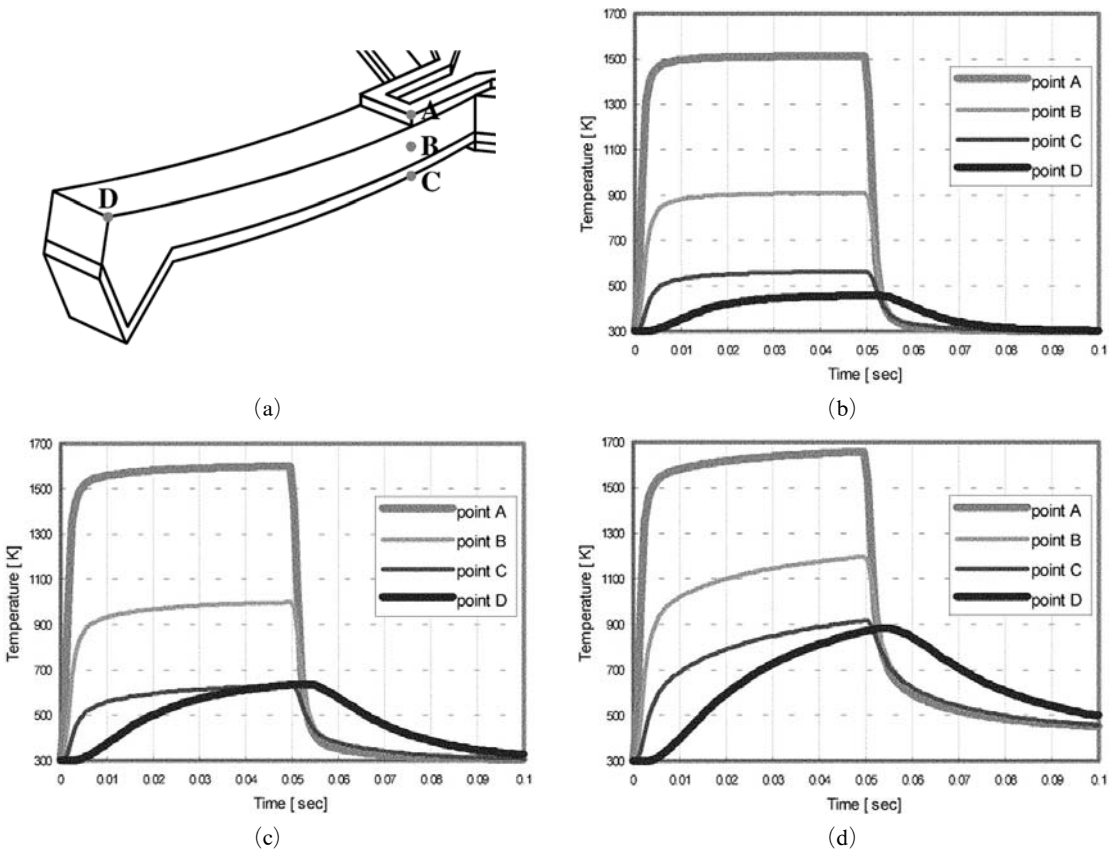

Fig. 7 Predicted time histories of temperature at the selected points (A~D)

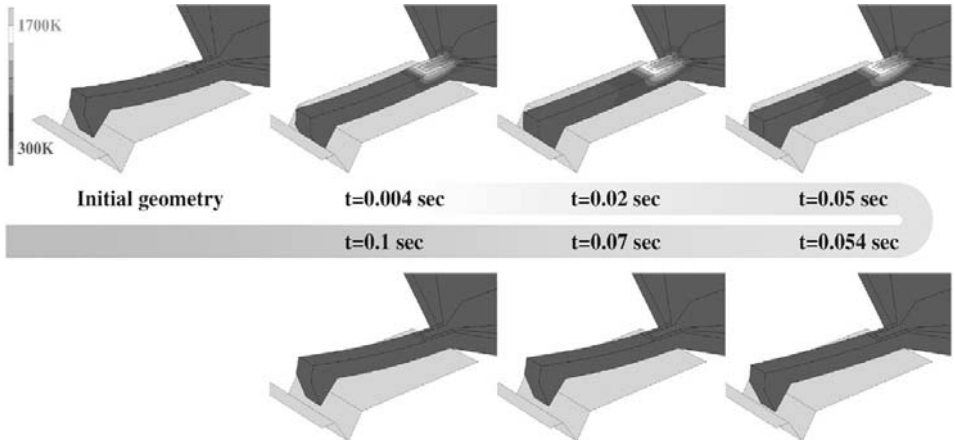

Fig. 8 Predicted temperature distributions on the thermally actuated probe

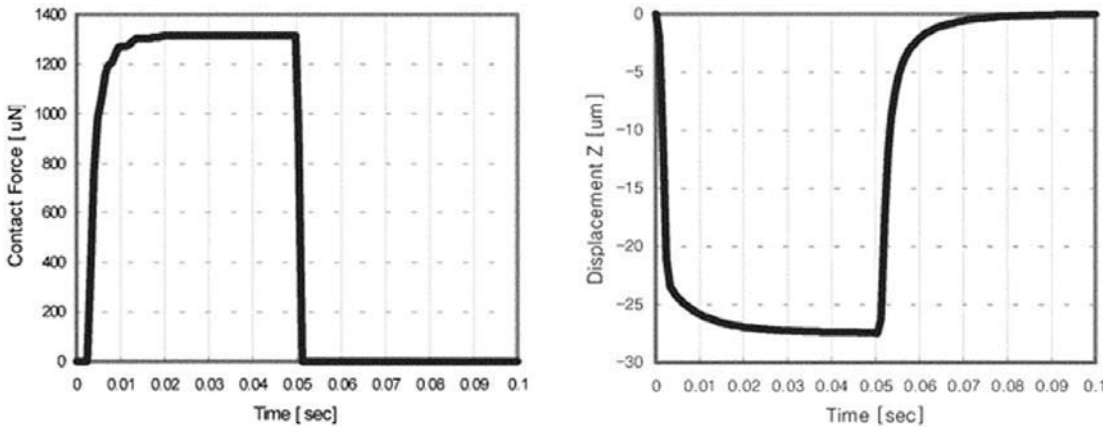

(a) Contact force (b) Displacement Z of the tip

Fig. 9 Predicted curves of contact force and displacement Z of the tip, vs. time, respectively

In case of thermally insulated system (Fig. 7(d)), heat is apt to be redistributed internally over initial temperature 300 K. The bimorph thermal actuator can realize one cycle for 0.1 sec perfectly. Figure 8 shows predicted temperature distributions in probe surface for respective time.

The temperature of probe tip which makes contact with biocell directly is very important. The maximum temperature of probe tip at steady state is around 456 K, and may give heat shock to biocell.

5.4.2 Force exerted by actuator

The contact force of probe and the Z-displacement of probe tip are shown in Fig. 9(a) and 9 (b) during 0.1 sec. In the first stage, when probe cantilever is bent down, the convex area of cantilever makes contact with an area between V-groove and probe body firstly. From this time, contact force increases until the whole system arrives at thermal steady state. The maximum contact force is around 1317 μN (~0.13 gf). On the other side, it is thought that probe tip makes contact with biocell firstly in case of real measurement.

6. Modification of Electrode and Temperature Measurement

6.1 Modified electrode model

It is shown that the bimorph thermal actuators can be optimized through changing the length of

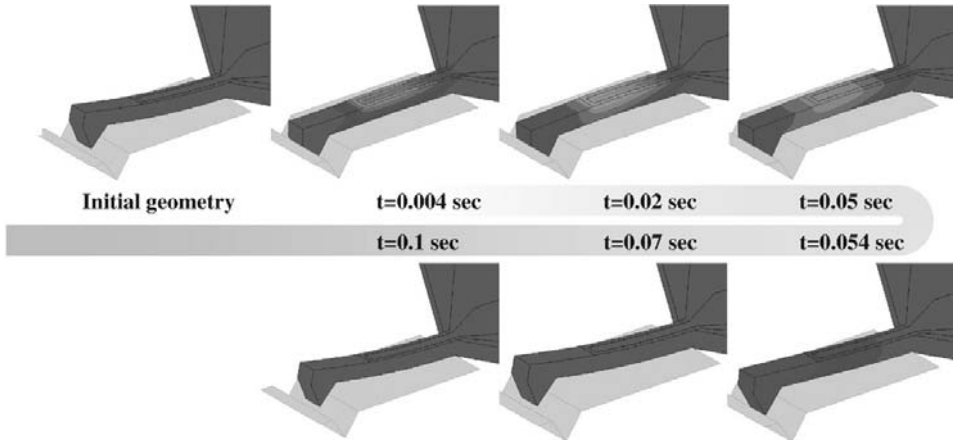

Fig. 10 Predicted temperature distributions on the thermally actuated probe for modified model

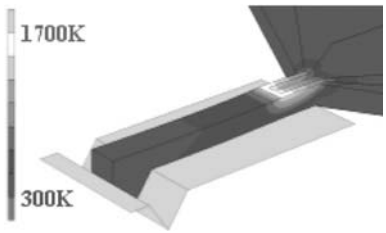

(a) Initial model

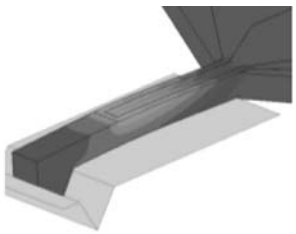

(b) Modified model

Fig. 11 Predicted temperature distributions on the thermally actuated probe at steady state

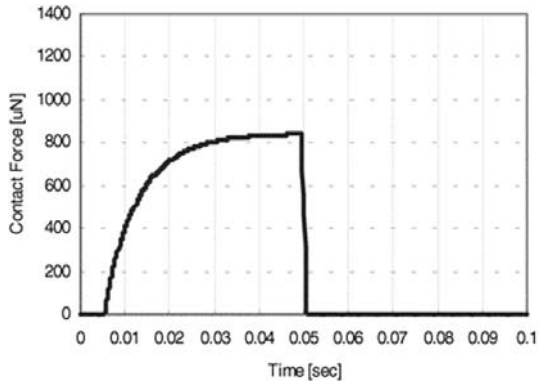

(a) Contact force

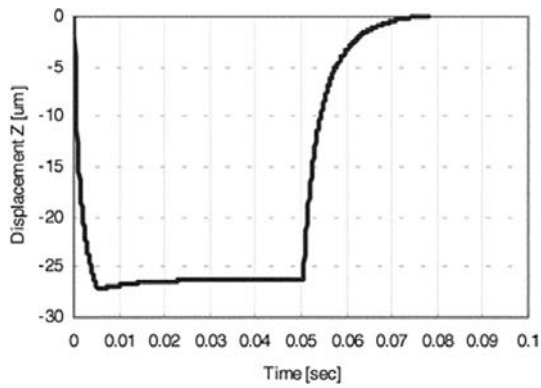

(b) Displacement Z of the tip

Fig. 12 Predicted curves of contact force and displacement Z of the tip, vs. time, respectively for modified model

electrode. Figure 10 shows predicted temperature distributions in probe surface for respective time. For modified electrode model, bimorph thermal actuator can also realize one cycle for 0.1 sec perfectly.

Figure 11 shows the predicted temperature distributions on the probe surface at steady state. The predicted maximum temperature of Au electrode in simulations with the initial and the modified model was 1513 K and 1130 K, respectively. Since 1513 K is excessive as compared with 1337 K, the melting point of pure Au, the length of Au electrode was modified from 50 μm to 150 μm in order to reduce a potential difference per unit length. This can certainly affect the shape of deflection with different temperature distribu-

tions. As shown in Fig. 11, the predicted maximum temperature of probe tip was around 456 K and 695 K in each model. Both may give heat shock to biocell. These results, however, show the feasibility of the optimization of the present probe system.

The predicted maximum contact force was around 841 μN at modified model as shown in Fig. 12. Also, the deflection pattern of the modified model is dissimilar from that of the initial model. The deflection pattern may be connected with the performance of electrical sensing.

6.2 Temperature measurement by infrared ray

When the cantilever beam was heated by flowing current in heater, it moved downwards. Input voltage up to 1.8 V could be supplied without damaging electrode by overheating. The practical temperature of probe tip was measured by two methods ; one is infrared rays' temperature measuring instrument (Keyence, model IT2-02), and the other is thermocouple. The temperature measured from both of them was around 30℃ as shown in Table 5. It was much lower than analytical temperature, which reached over 200℃. This is due to the fact that the infrared rays' temperature measuring instrument has a focus point of 1.2 mm diameter, and so the measured temperature indicates the average value including the surroundings of probe and the sensing part in SU-8/poly-silicon probe, not the temperature spread over probe tip. Even though it is averaged value due to the wide focal region of the instrument, this experimental result means that the temperature of sensing part is low enough that the bimorph probe almost never gives cells thermal damages during the characterization of cells (Ataka et al., 1993).

Table 5 Temperature data of probe tip measured with infrared rays' temperature measuring instrument

	Voltage	Current	Average Temperature
Experiment 1	1.0 V	24 mA	26.5℃
Experiment 2	1.4 V	30 mA	30.2 ℃

The practical current level in Table 5 was almost same as the analytical current level (30~40 mA). Moreover, even the bimorph actuated sensing probe cannot generate large force, the force range is compatible with what a biological cell withstands without any damage, and displacement of probe is large enough to characterize a biocell in the microfluidic channel.

7. Conclusions

In this paper, a novel structure for a single-cell characterization is proposed which makes use of a bimorph actuated sensor arrays with integrated microfluidic channels. Understanding about the actuation of bimorph actuated probe and investigation of physical phenomena by heat transfer is achieved using finite element analysis methods. Through virtual simulation, the author could predict not only deflection of cantilever before and after release, but also temperature distribution and contact force.

Heat loss by radiation is neglected, because it is very small when compared with heat emission by conduction or convection. The temperature range to be considered in this research is from 300 K to 1600 K. The effect of convection in heat transfer from Au electrode to surroundings has consequence about 1~2%. However, it is positively necessary to consider the effect of convection in actuation analysis of bimorph thermal actuator, when analyzed from time which it takes to be steady state, and thermal and mechanical responses.

Under the rational assumptions with restricted information about material physical responses and process conditions at very high temperature and very small scale, it is predicted that this bimorph thermal actuator can realize one cycle for 0.1 sec perfectly from Joule-heat-mechanical coupling analysis.

The contact force and temperature of probe tip which makes contact with biocell directly were predicted to be 0.13 gf and 160℃ at steady state, respectively. The predicted contact force level is proper for characterization of biocell, but the predicted temperature of probe tip may give seri-

ous damage to biocell.

The maximum temperature of Au electrode at steady state which is predicted by virtual simulations is 1513 K, and it is very high temperature compared with melting point of pure Au (1337 K). It is necessary to reanalyze this problem based on analysis model proper to micro scale problem as well as more exact material properties and analysis method. However, we confirmed that it is possible to get more information about characteristics of bimorph thermal actuator through present analysis. On the other hand, comparison with real phenomena and calibration is necessary in order that virtual simulations are good tools of optimization eventually. Therefore, measurement of exact temperature at local area with micro-scale resolution is necessarily required.

In modified model, the predicted maximum contact force is around 841 μN, and the predicted maximum temperature of Au electrode in simulations with the modified model is 1130 K. Also, the predicted maximum temperature of probe tip is around 695 K.

Bimorph actuated microsensor has a three-dimensional movable microsensor with vertical probe actuation. Therefore, cells can be isolated from the planar environment by bimorph thermal actuator, so the electrical property as well as mechanical property of cell can be characterized in single level in aqueous media.

In the future works, the complete system including channels, signal sensing electrodes and circuits, packaging or fluidic sealing, etc, will be optimized and fabricated. Then the electrical characterization of single living cell will be investigated beyond aqueous media. To characterize the mechanical properties of cell, such as cell membrane, interaction between cells, piezoresistive sensor or optical lever method can be integrated to the present bimorph cantilevers as well as electrical elements. Finally, the proper method for real fluidic sealing should be developed for real measurement of a single cell.

Acknowledgments

This work is carried out within CIRMM-CNRS framework between IIS, The University of Tokyo and IEMN-CNRS, for the collaboration project. The author would like to thank all members of silicon micro system group and clean-room staffs in IIS and IEMN.

References

Ataka, M., Omodaka, A., Takeshima, N. and Fujita, H., 1993, "Fabrication and Operation of Polyimide Bimorph Actuators for a Ciliary Motion System," *IEEE Journal of Microelectromechanical Systems*, Vol. 2, pp. 146～150.

Chronis, N. and Lee, L. P., 2004, "Polymer MEMS-based Microgripper for Single Cell Manipulation," *Proc. IEEE Micro Electromechanical Systems Workshop*, pp. 17～20.

Fadmacher, M., 1997, "Measuring the Elastic Properties of Biological Samples with the AFM," *IEEE Engineering in Medicine and biology*, Vol. 16, pp. 47～57.

Incropera, F. P. and De Witt, D. P., 1990, *Introduction to Heat Transfer*, 2nd Edition, John Wiley & Sons.

Kim, B. J., Collard, D., Lagouge, M., Conseil, F., Legrand, B. and Buchaillot, L., 2003, "Thermally Actuated Probe Arrays for Manipulation and Characterization of Individual Bio-cell," *Proc. of the 12th. Int. Conference on Solid-State Sensors, Actuators and Microsystems*, Vol. 2, 3E22.P, pp. 1255～1258.

Kim, N., Lee, J., Seo, T. and Kim, C., 2002, "Combined Convection and Radiation in a Tube with Circumferential Fins and Circular Disks," *KSME International Journal*, Vol. 16, No. 12, pp. 1725～1732.

Pichonat-Gallois, E. and Labachelerie, M., 2003, "Thermal Actuators Used for a Micro-optical Bench : Application for a Tunable Fabry-perot Filter," *Proc. of the 12th. Int. Conference on Solid-State Sensors, Actuators and Microsystems*, pp. 1419～1422.

Vargaftik, N. B., 1956, *Teplofizicheskiye Svoystva Veshchestv* (*Thermophyical Properties of Substances*), Reference Book, Gosenergoizdat, pp. 142～143.

Weast, R. C., Astle, M. J. and Beyer, W. H.,

2003, *Handbook of chemistry and physics*, 84th Edition, CRC Press.

Yu, C. C. and Yang, Y. J., 2003, "Extraction of Heat Transfer Macromodels for MEMS devices," *Proc. of the 12th. Int. Conference on Solid-State Sensors, Actuators and Microsystems*, pp. 1852~1855.